Research on Engineering Structures & Materials
www.jresm.org
Research Group

Research Article

Enhancing open capacity in active distribution networks via GBD-based network reconfiguration considering PV integration constraints

Ruohui Mo [*,a], Yangyu Dai [b], Jialin Song [c], Hanchang Huang [d], Jun Wang [e], Shounan Lin [f], Minglong Zou [g]

Power Dispatching and Control Center, Hainan Power Grid Co., Ltd., Haikou 570000, China

Article Info

Article History:

Received 14 July 2026

Accepted 25 Aug 2026

Keywords:

Proactive distribution networks; Open capacity assessment; Generalized Benders Decomposition; Feasible cut generation; N–1 security constraints; Distributed photovoltaics

Abstract

As the penetration rate of distributed photovoltaic (PV) systems continues to rise, the power fluctuation, reverse power flow, and node voltage constraint challenges within active distribution networks have increased significantly. This makes traditional open capacity assessment methods—based on fixed operating conditions—less effective at accurately capturing the dynamic impact of PV integration on the network's load-bearing capacity, thereby presenting new challenges for both open capacity assessment and enhancement efforts. To address this challenge, this study proposes a proactive distribution network openable capacity model that incorporates constraints arising from distributed photovoltaic (PV) integration. The model integrates multiple components, including node power flow, voltage deviation, line capacity, reverse power flow, and N–1 security constraint. Building upon this framework, the proposed approach employs the generalized Benders decomposition method (GBD) combined with the feasible cut generation method (FCG) to solve the constructed hybrid integer nonlinear optimization model. Specifically, GBD is utilized to decompose the complex optimization problem, while FCG reduces the search space by screening infeasible regions and generating effective constraints, thereby enhancing the computational efficiency of the model. Experimental results from the IEEE 33-node active distribution network test system demonstrate that the maximum open capacity reaches 7.8 MW, with an 18.2% increase after optimization. The average and peak load rates decrease from 67.2% to 43.6% and from 89.4% to 54.8%, respectively. Under extreme load scenarios, the maximum open capacity reaches 10.7 MW with a calculation time of 10.8 seconds. The proposed method improves capacity assessment and reconfiguration performance, supporting photovoltaic integration and safe distribution network operation.

1. Introduction

The high penetration of distributed photovoltaic (PV) systems has altered the unidirectional power flow characteristics of traditional distribution networks, gradually transforming them from unidirectional power supply networks into active distribution networks characterized by coordinated interaction among generation, grid, and load. Under conditions of high PV penetration, fluctuations in PV output exacerbate the occurrence of bidirectional power flows within distribution networks, thereby giving rise to additional challenges such as node voltage deviations, increased line capacity constraints, and difficulties in accurately assessing available open capacity.

*Corresponding author: Ruohui_Mo@outlook.com
[a]orcid.org/0009-0005-0284-5650; [b]orcid.org/0009-0003-9333-4471; [c]orcid.org/0009-0007-0472-5809; [d]orcid.org/0009-0005-3294-5425; [e]orcid.org/0009-0005-8569-210X; [f]orcid.org/0009-0008-0897-8720; [g]orcid.org/0009-0006-8706-4753
DOI: http://dx.doi.org/10.17515/resm2026-1871vk0714rs

Open capacity, as an important indicator of the distribution network's ability to accommodate new loads or distributed power sources, is directly related to photovoltaic grid connection planning, user installation review, and distribution network expansion decisions [1-2]. The concept of Open Capacity is related to Hosting Capacity, as both describe a distribution network's ability to accommodate additional distributed energy resources under operational constraints. However, while Hosting Capacity generally refers to the maximum DG integration level, this study defines Open Capacity as the remaining margin available for new PV integration under the current topology, security constraints, and operating conditions, excluding load-bearing capacity. In high-PV-penetration scenarios, open capacity is jointly constrained by transformer capacity, line thermal limits, PV output fluctuations, voltage deviations, reverse power flow, and network topology. Increased PV output changes power flow distribution and may cause local nodes to export power, leading to voltage rise and flow reversal. As PV penetration further increases, voltage limits may become the dominant constraint, thereby restricting additional PV integration and open-capacity enhancement. Therefore, constructing an open capacity assessment and optimization reconfiguration method oriented to distributed photovoltaic access constraints is of great significance for enhancing photovoltaic consumption capacity and operational safety. For example, Othman et al. constructed a distributed power access capacity assessment model considering node voltage constraints and verified the limiting effect of voltage margin on access capacity through distribution network examples [3]. Lu et al. proposed a calculation method for photovoltaic acceptance capacity based on probabilistic power flow, introducing light randomness and load uncertainty into the capacity assessment process. This method could reduce the risk of capacity overestimation brought by the static assessment model [4]. Tian et al. used sensitivity analysis to identify key nodes for photovoltaic access and established an access capacity optimization model oriented to line capacity constraints. This method could improve the interpretability of node access schemes [5]. Liu et al. considered reverse power flow and voltage over-limit problems and proposed a multi-constraint capacity assessment framework, which demonstrated good operational safety in multiple test systems [6]. Yang et al. analyzed node voltage deviations under different photovoltaic penetration rates in combination with actual distribution network operation data. Photovoltaic access location had a significant impact on open capacity [7]. However, existing studies on open capacity assessment primarily focus on static constraints such as node voltages, line capacities, and uncertainties in photovoltaic (PV) output; these studies typically perform capacity calculations based on fixed network topologies and fail to adequately account for the role of dynamic topology adjustments within active distribution networks in enhancing capacity. Consequently, in scenarios featuring high penetration levels of distributed PV generation, relying solely on static assessment methods is insufficient to further explore the potential capacity enhancement achievable through network reconfiguration.

With the development of active distribution network operation control technology, network reconfiguration has gradually become an important means to increase open capacity and improve the operation status of distribution networks [8]. Elumalai et al. employed the particle swarm optimization algorithm to optimize the switching states of distribution networks incorporating distributed generation; the results demonstrated that this method can reduce line losses, but is prone to convergence fluctuations under complex constraints [9]. The generalized Benders decomposition (GBD) approach adopted in this paper decomposes the discrete topology decision-making and continuous power flow constraints through iterative interaction between the master problem and subproblems; it utilizes the objective value of the master problem to establish a lower bound and employs the feedback results from the subproblems to form an upper bound, thereby assessing the optimization process via the gradual convergence of these bounds, thus avoiding the convergence instability issues inherent in stochastic search from a mathematical perspective. Oni et al. proposed a distribution network reconfiguration model based on mixed integer second-order cone programming, which convexified the power flow constraints and improves the solvable model [10]. Chowdhury et al. used Generalized Benders Decomposition (GBD) to handle the coupling problem of switching variables and continuous power flow variables, and reduced the difficulty of solving the mixed-integer nonlinear model through master-slave problem interaction [11]. Khodr et al. proposed an optimal power flow (OPF)-based distribution network reconfiguration method that incorporates Benders decomposition into the network reconfiguration solution process; by leveraging information exchange between the master problem and subproblems to handle the coupling relationship between discrete switch variables and continuous power flow variables, this approach enhances the computational efficiency of solving complex distribution network optimization problems [12]. Tavagnutti et al. combined distributed photovoltaic output prediction with topology adjustment strategies to verify the role of network reconfiguration in enhancing photovoltaic consumption capacity and reducing operational risks [13]. In summary, existing methods for open capacity assessment and active distribution network reconfiguration still exhibit certain limitations when addressing scenarios with high penetration of distributed photovoltaic (PV) generation. On one hand, some capacity assessment models only consider static loads or a single voltage boundary, making it difficult for them to simultaneously reflect the comprehensive impact of PV output fluctuations, line capacity constraints, and reverse power flow on the available open capacity; on the other hand, existing network reconfiguration methods typically prioritize optimization objectives such as reducing network losses, improving load balancing, or enhancing operational economic efficiency, focusing more on optimizing the current operating state rather than setting increasing the acceptance capability of distributed PV generation or expanding the available open capacity as their core objective. Therefore, how to achieve synergy between capacity assessment and capacity enhancement through network topology optimization remains an urgent challenge for active distribution networks with high PV penetration.

To address the aforementioned issues, this paper proposes an active distribution network-based method for evaluating openable capacity and performing optimal topology reconstruction that incorporates constraints arising from distributed photovoltaic (PV) integration. Unlike traditional capacity evaluation methods based on fixed network topologies, this approach treats the network topology as an adjustable variable, thereby extending the openable capacity evaluation process from static boundary calculations to a dynamic capacity optimization problem oriented toward active network reconstruction. At the solution level, the Generalized Benders Decomposition (GBD) method is employed to decompose the discrete switch decisions and the continuous nonlinear power flow constraints; furthermore, a Feasible Cut Generation (FCG) mechanism is introduced to linearize the voltage violation and line overloading information detected in the subproblems into feasible cuts and feed these back to the master problem, thereby actively eliminating infeasible topology regions. This framework establishes a closed-loop solution mechanism comprising "capacity evaluation – topology optimization – power flow verification – feasible region correction," which enhances the capacity for integrating new PV generation while reducing ineffective search processes. The main contributions of this paper are as follows:

- Develop an open-capacity assessment model that accounts for distributed photovoltaic (PV) output fluctuations, voltage constraints, line capacity constraints, and the impact of reverse power flow, thereby enhancing the accuracy of capacity assessment in scenarios with high PV penetration.
- Establish an active distribution network optimization and reconfiguration model oriented toward capacity enhancement, which integrates the maximization of available open capacity with the minimization of system losses within a unified optimization framework, and employs a weighting mechanism to reconcile the conflicts between these objectives and operational economic efficiency.
- This paper proposes a collaborative solution method based on Generalized Benders Decomposition (GBD) and the Feasible Cut Generation (FCG) mechanism. Within this framework, the FCG mechanism generates valid cut constraints based on infeasibility information such as voltage violations and line overloads, actively excludes invalid search regions, and shrinks the search space of the optimization problem, thereby enhancing the solution efficiency for complex mixed-integer nonlinear models.
- The effectiveness of the proposed method is verified using the IEEE 33-node active distribution network test system, and its overall performance in enhancing the integration capability of distributed photovoltaics, reducing operational losses, and ensuring system security is analyzed.

2. Materials and Methods

When distributed photovoltaic (PV) systems are integrated at a high penetration level, the power flow direction of the distribution network, the node voltage distribution, and the line load conditions will all undergo dynamic adjustments in response to changes in the network topology. The issue of increasing available capacity is not only influenced by electrical operational constraints but also exhibits significant complexity due to the diversity of possible network topologies. Therefore, it is necessary to integrate network reconfiguration strategies with capacity assessment to achieve synergy between topology optimization and the enhancement of PV integration capability.

2.1. Open Capacity Modeling for Active Distribution Networks Considering Distributed Photovoltaic Access Constraints

The large-scale access of distributed photovoltaic has gradually shifted the active distribution network from the traditional unidirectional power supply mode to the source-grid-load coordinated operation mode. Due to the randomness, volatility, and uneven spatiotemporal distribution of photovoltaic output, when a large number of photovoltaic cells are connected to the same area, it is easy to cause problems such as node voltage over-limit, line reverse power flow and local equipment overload, thereby causing large errors in the assessment results of open capacity based on static load growth [14-15]. Therefore, the study first constructs the distributed photovoltaic access structure model of the active distribution network, as illustrated in Figure 1.

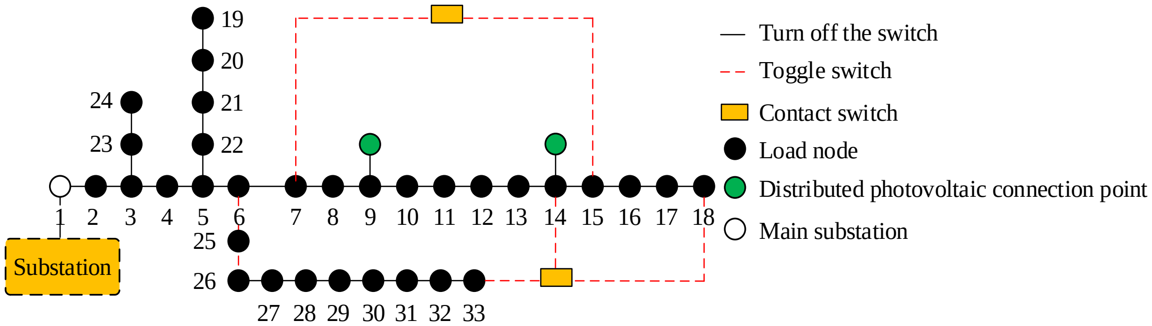

Fig. 1. Integration architecture of IEEE 33 active distribution network with distributed photovoltaic systems

As shown in Figure 1, the substation serves as the main power source supplying power to various feeder lines, with multiple photovoltaic (PV) units connected to different nodes to form a multi-source power supply structure. Given that open capacity assessment focuses on determining the maximum additional PV capacity that the system can accommodate under safety constraints, this study employs the PV peak generation and the most adverse operating conditions under low-load scenarios for analysis. When the PV output reaches its peak value, power backflow may occur in certain areas, leading to an increase in node voltage; simultaneously, under low-load conditions, the proportion of PV output further increases, making the risks of reverse power flow and voltage exceedance more pronounced. When the PV output decreases, the system still relies on the main substation to maintain power balance [16-17]. Therefore, the available open capacity is not only related to the level of load growth but is also jointly influenced by the scale of PV integration, operating conditions, and the connection location. To quantify the impact of PV integration on the node power distribution, this study defines the node net injection power as shown in Equation (1). Here, the research object is an active distribution network incorporating distributed PV resources, without considering other controllable distributed energy sources such as energy storage or batteries; consequently, the node power balance model includes only three primary power variables: the power supplied by the substation, the PV output power, and the node load power. If other distributed energy sources are present, their output power can be uniformly incorporated into the distributed energy injection term.

$$P_i^G + P_i^{PV} - P_i^L = V_i \sum_{j=1}^{N} V_j (G_{ij} cos\theta_{ij} + B_{ij} sin\theta_{ij}) \tag{1}$$

In Equation (1), P_i^G represents the active power supply provided by the substation to node i; P_i^{PV} represents the active power injected by distributed photovoltaic systems at the node; P_i^L represents the power consumed by the node load. V_i and V_j signify node voltage amplitudes. G_{ij} and B_{ij} signify the conductance and admittance of the node admittance matrix. θ_{ij} represents the phase angle difference of the node. This analysis does not further consider other distributed energy sources such as energy storage; their role may be expanded to include the distributed power injection component based on actual requirements. The corresponding reactive power balance relationship is represented in Equation (2).

$$Q_i^G + Q_i^{PV} - Q_i^L = V_i \sum_{j=1}^{N} V_j (G_{ij} \sin\theta_{ij} + B_{ij} \cos\theta_{ij}) \tag{2}$$

In Equation (2), Q_i^G, Q_i^{PV}, and Q_i^L respectively represent the reactive power support power of the substation, the reactive power injection power of the photovoltaic system, and the reactive power demand of the node load. Since this paper mainly focuses on the impact of distributed photovoltaic integration on the open capacity of the active distribution network, no additional adjustable reactive power equipment such as energy storage inverters are introduced. Moreover, in order to quantify the acceptance capacity of the active distribution network for the newly added distributed photovoltaic under the safety operation constraints, the study introduces the photovoltaic integration capacity growth coefficient λ, and the objective function is expressed as Equation (3).

$$maxF = \lambda \sum_{i=1}^{N} P_i^{pv} \tag{3}$$

In Equation (3), F represents the maximum openable capacity of the system, which is the additional distributed photovoltaic capacity that the active distribution network can further accommodate under the constraints of node voltage, line transmission, and N-1 safety; λ represents the load growth coefficient. This paper focuses on the capacity improvement issue under the condition of distributed photovoltaic grid connection, so the increase in new load is not taken as the object for defining the openable capacity. After completing the node power flow modeling, the study constructs an open capacity assessment model considering distributed photovoltaic access constraints, whose structure is shown in Figure 2.

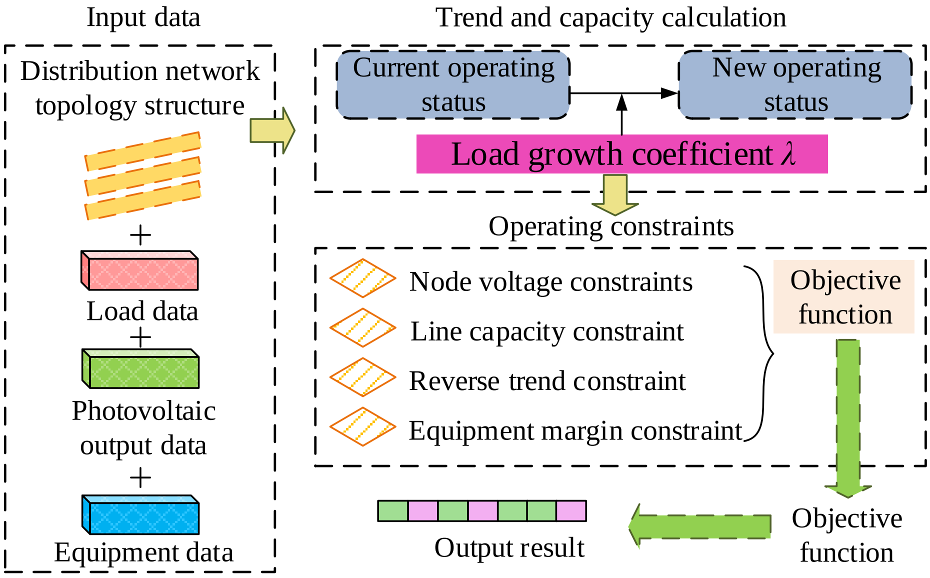

Fig. 2. Open capacity assessment model

In Figure 2, the open capacity is mainly constrained by four parts: photovoltaic access capacity, voltage regulation capacity, line transmission capacity and equipment operating margin. When the photovoltaic access capacity exceeds a certain critical value, the system will first be restricted by voltage constraints and then by line capacity constraints. To ensure the operational safety of nodes, this study investigates the development of a node voltage constraint model. Given that the scale of photovoltaic (PV) integration, network topology, and operating conditions in an active distribution network all influence the voltage response characteristics of nodes, this paper employs a sensitivity analysis method based on the Jacobian matrix to compute the relationship between node voltages and variations in PV output; furthermore, during each optimization iteration, the sensitivity matrix is updated according to the current operating conditions to enhance the adaptability of the constraint model for large-scale network scenarios. The corresponding expression is presented in Equation (4).

$$V_i^{min} \leq V_i + \frac{\partial V_i}{\partial P_i^{PV}} \Delta P_i^{PV} \leq V_i^{max} \tag{4}$$

In Equation (4), $\frac{\partial V_i}{\partial P_i^{PV}}$ represents the sensitivity coefficient of the node voltage to the variation of photovoltaic output. ΔP_i^{PV} represents the increment of photovoltaic output. $V_i^{\min}$ and V_i^{max} signify the upper and lower limits of voltage. Since this constraint model is based on the local linearization assumption, it introduces a certain degree of linearization error. Therefore, during the subsequent optimization and reconstruction process, the study employs nonlinear power flow calculations within the GBD subproblem to precisely validate the output results of the master problem, and utilizes FCG to generate corrected cutting constraints based on voltage limit violations, thereby gradually eliminating the infeasible region caused by the linearization error. Meanwhile, to avoid line overload, the line capacity constraint is shown in Equation (5).

$$\sqrt{\left(P_{ij}\right)^2 + (Q_{ij})2} \leq S_{ij}^{max} \tag{5}$$

In Equation (5), P_{ij} and Q_{ij} signify the active power and reactive power of the line, respectively. S_{ij}^{max} represents the maximum allowable transmission capacity of the line. This constraint can ensure that the line operation is always within the thermal stability range. Based on the above, the voltage over-limit and reverse power flow safety constraint model is constructed, and the relationship is shown in Figure 3.

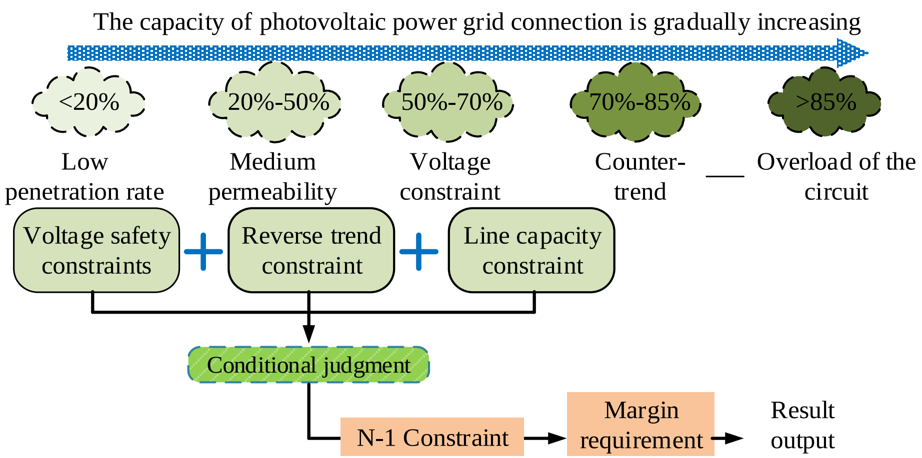

Fig. 3. Voltage and reverse power flow safety constraint model

In Figure 3, when the photovoltaic access capacity gradually increases, the system is first constrained by the node voltage. As the photovoltaic capacity continues to increase, some feeders start to show reverse power flow. If the scale of access is further increased, the line load rate and the safety margin for equipment operation will continue to decline. Therefore, considering only load growth capacity while ignoring network security constraints will result in significantly larger capacity assessment outcomes. To ensure that the system can still operate stably in the event of a failure, the study further introduces N-1 security constraints as shown in Equation (6) [18-19]. In this study, to account for the changes in the system's operating conditions resulting from the outage of different faulty lines or equipment, normalized indices are employed to describe the power flow variations and node voltage deviations under fault conditions; specifically, the rated transmission capacity and rated voltage of each line are used as the respective normalization bases, thereby eliminating the influence arising from differences in line capacity ratings and node voltage levels.

$$max\left(\frac{|S_{ij}^k|}{S_{ij}^{max}}()\, max\left(\frac{|V_i^k - V_i^{ref}|}{V_i^{ref}}\right)\right) \tag{6}$$

In Equation (6), S_{ij}^k represents the apparent power flow of line $i-j$ under the kth fault scenario; S_{ij}^{max} represents the maximum transmission capacity of line $i-j$, which is used for normalization processing of the line flow in the fault state; V_i^k represents the voltage amplitude of node i under the kth fault scenario; V_i^{ref} represents the rated voltage of node i, which is used for normalization processing of the node voltage deviation; ε represents the system safety margin threshold, which is used to limit the line load level and node voltage deviation degree in the fault state. In this paper, ε = 0.15 is set, indicating that in the N-1 fault situation, the comprehensive normalized index of line flow and node voltage deviation does not exceed 15%, that is, the system still retains 85% of the safety operation margin, to ensure that the active distribution network has the stable operation capability after a single component fault.

2.2. Active Distribution Network Optimization Reconfiguration Methods for Available Integration Capacity Enhancement

After completing the open capacity modeling, the study further proposes optimization and reconfiguration methods for active distribution networks to enhance the open capacity and safety margin of the system under distributed photovoltaic access conditions. Due to the large number of switch, line and node constraints in active distribution networks, the system operation is highly nonlinear, and traditional single-step optimization is difficult to simultaneously satisfy the requirements of capacity maximization and safety stability [20]. The study synergistically optimizes capacity enhancement and network security by constructing an active distribution network optimization reconfiguration model, introducing distributed photovoltaic access constraints, node voltage constraints and line load constraints. The overall process is shown in Figure 4.

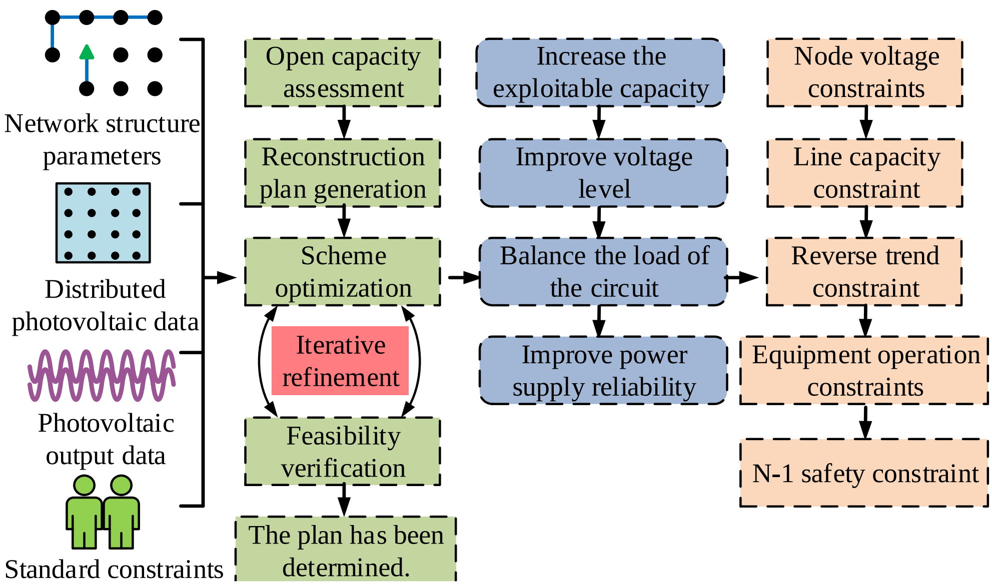

Fig. 4. Framework for active distribution network optimization and reconstruction

In Figure 4, the system first builds the initial network topology given photovoltaic access capacity and node load, then calculates the upper limit of open capacity through the optimization model, and adjusts the network switching state according to node voltage, line load and N-1 safety constraints to achieve network reconstruction. The study defines the optimization objective function as a combined objective of maximizing available integration capacity and minimizing system loss, and its calculation is shown in Equation (7). Within the GBD solution framework, Equation (7) serves as the optimization objective of the main problem, primarily responsible for determining the network switch states and topology configuration to enhance openable capacity; meanwhile, continuous constraints such as power flow calculations, voltage deviations, and line security verification are solved via subproblems, and feedback constraints are generated based on the results of these subproblems.

$$max\, Z = \omega_1 \sum_{i=1}^{N} P_i^{PV} - \omega_2 \sum_{(i,j)\in L} R_{ij} I_{ij}^2 \tag{7}$$

In Equation (7), Z represents the comprehensive optimization objective. ω_1 and ω_2 are the capacity weight and loss weight coefficients, respectively. R_{ij} and I_{ij} are line resistance and line current, respectively. L is the collection of lines. Since capacity enhancement and loss reduction may conflict, this study adopts a normalized weighted objective. Capacity enhancement is assigned a higher weight as the primary goal, while network loss serves as an auxiliary economic objective. Sensitivity analysis is conducted for different weight combinations, and the combination with the best overall performance is selected for subsequent experiments.

To address this nonlinear mixed integer programming problem, this study introduces the GBD method, whose structure is illustrated in Figure 5 [21]. Compared with the commonly used Second-Order Cone Programming (SOCP) approach, the GBD method does not require an overall convexification of the original nonlinear power flow constraints; instead, it preserves the original physical characteristics of the voltage constraints, line power flow constraints, and N–1 security constraint in active distribution networks.

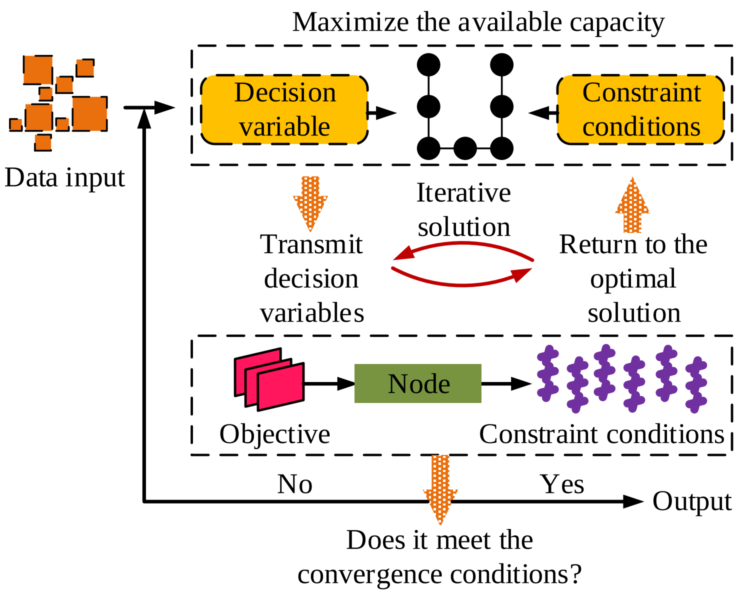

Fig. 5. Generalized benders master-subordinate coordination optimization structure

As shown in Figure 5, the main problem is responsible for optimizing the switching state of the network, generating preliminary solutions by relaxing capacity constraints and voltage constraints. The sub-problems are responsible for power flow calculation and feasibility check, calculating node voltage and line power flow based on the switch state output by the main problem, and generating feasible cut constraints to feed back to the main problem. Through the interaction and iteration of the master and sub-problems, the system can gradually increase the open capacity while meeting the constraints. In the subproblem, the node voltage is calculated using a nonlinear power flow model, as shown in Equation (8). Given that active distribution networks typically maintain a radial power supply structure through the control of tie-switches during actual operation, this paper assumes that the optimized reconfigured network still satisfies the radial topology constraints. Under these conditions, the node voltage drop relationship can be described using a model analogous to the DistFlow model, thereby reducing the computational complexity of the power flow calculation and meeting the iterative solution requirements for the GBD subproblem.

$$V_i = V_j + \sum_{(i,j)\in L} (R_{ij}P_{ij} + X_{ij}Q_{ij}) \tag{8}$$

The line flow calculation is shown in Equation (9).

$$\theta_i - \theta_j = arctan\left(\frac{X_{ij}P_{ij} - R_{ij}Q_{ij}}{V_iV_j}\right) \tag{9}$$

In Equation (9), θ_i and θ_j represent the phase angle of the node voltage. R_{ij} and X_{ij} represent line resistance and reactance, respectively. Since the research focus of this paper is on active distribution network reconfiguration scenarios, the network topology adjustment process must satisfy radial constraints; therefore, Equations (8) and (9) are applicable to the reconfigured radial operating structure. For mesh-type distribution systems that operate in closed-loop mode, a complete AC power flow model must be further employed for the calculations. To speed up the iterative convergence, the study introduces FCG into the main problem, and the process is shown in Figure 6.

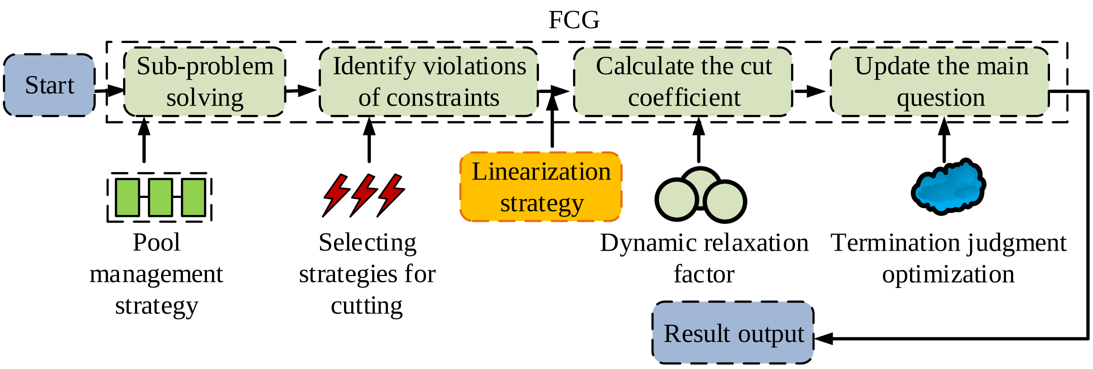

Fig. 6. Generation of feasible cuts and mechanisms for accelerated convergence

As shown in Figure 6, the feasible cut generation module checks the feasibility of the subproblem after each iteration. When constraints such as node voltage limits violation or line overloading are detected, the system linearizes the violated constraints based on the current iteration results and generates feasible cut constraints to be fed back to the GBD master problem, thereby eliminating the current infeasible search region and narrowing the subsequent optimization space. The pseudocode of Algorithm 1 is as follows:

1: Initialize iteration counter k=0;

2: Initialize switching variables xk=x0;

3: Set upper bound UB=+∞ and lower bound LB=-∞;

4: Initialize feasible cut set Ω=∅;

5: Construct the master problem:

max F(x)

subject to Ω

6: while $|UB-LB|/|UB| > \varepsilon$ and $k < K_{max}$ do

7: Solve the master problem and obtain the optimal switching state xk;

8: Update the network topology according to xk;

9: Calculate photovoltaic hosting capacity and power loss objective value;

10: Update upper bound:

$UB=\max\{UB,F(xk)\}$;

11: Construct the subproblem with fixed topology xk;

12: Perform AC power flow calculation;

13: Calculate node voltage U_i and line power flow S_{ij};

14: if

$U_{i,min} \le U_i \le U_{i,max}$

and

$S_{ij} \le S_{ij,max}$

and

N-1 safety constraints are satisfied

then

15: Calculate subproblem objective value;

16: Update lower bound:

$LB=\max\{LB,F_{sub}(xk)\}$;

17: Record current optimal solution $x^*=xk$;

18: else

19: Identify violated constraints;

20: Generate feasible cuts based on voltage violation and line overload:

$g(xk)+\nabla g(xk)(x-xk)\le 0$

21: Add generated cuts into master problem:

$\Omega=\Omega\cup\{gcut\}$;

22: end if

23: Update iteration counter:

$k=k+1$;

24: end while

25: Return x* and Popen*;

Specifically, if in the k -th iteration the violation number of constraints detected by the sub-problem is $g(x)$, then the feasible cut constraint is expressed as shown in Equation (10).

$$g(x^k) + \nabla g(x^k)(x - x^k) \le 0 \tag{10}$$

In Equation (10), x represents the decision variable for the network switch status in the main problem; x^k represents the switch status obtained in the kth iteration; $g(x^k)$ represents the degree of constraint violation of the sub-problem under the current iteration; $\nabla g(x^k)$ represents the first-order gradient information of the constraint function at the current iteration point. This feasible cut transforms the infeasible information such as voltage over-limit and line overload in the sub-problem into the constraints of the main problem through local linearization. This enables the GBD algorithm to gradually eliminate the infeasible topological regions and improve the search efficiency. In the final capacity enhancement phase, the study constructs an integrated open capacity optimization process, whose structure is shown in Figure 7.

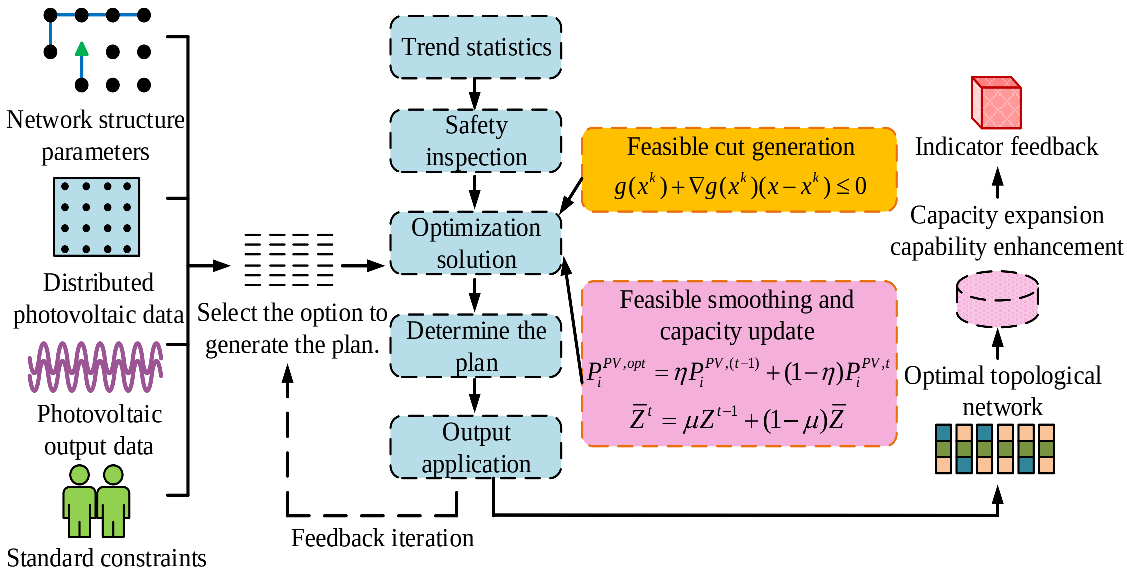

Fig. 7. Process for optimizing open capacity enhancement

In Figure 7, the system first calculates the upper limit of open capacity based on the initial network state, then iteratively adjusts the network switching state through GBD, while verifying the power flow of the sub-problem to ensure that the node voltage and line power flow meet the safety constraints. When the iteration converges, output the optimal network topology and the corresponding available integration capacity value. To mitigate significant fluctuations in capacity optimization results caused by network topology adjustments during the GBD iteration process, this study introduces a capacity sensitivity coefficient and an iterative smoothing coefficient to perform a weighted fusion of historical iteration results and the current optimization result; the corresponding calculation formula is given in Equation (11). In this formulation, the correlation coefficient remains constant throughout the optimization process, allowing the use of preset parameters to adjust the trade-off between historical information and the current search results, thereby ensuring stable convergence of the iterative process.

$$\begin{cases} P_i^{PV,opt} = \eta P_i^{PV,(t-1)} + (1-\eta) P_i^{PV,(t)} \\ \quad Z^{(t)} = \mu Z^{(t-1)} + (1-\mu) Z^{(t)} \end{cases} \tag{11}$$

In Equation (11), $P_i^{PV,opt}$ represents the optimized photovoltaic access capacity. $Z^{(t)}$ represents the optimization target value for the t -th iteration. In this paper, both parameters are set as fixed values, and their appropriate values are determined during the experimental phase through a parameter sensitivity analysis. In addition, to ensure that the network reconstruction results take both capacity and security into account, the study constructs an overall constrained optimization function, as shown in Equation (12).

$$L_{opt} = \alpha L_{volt} + \beta L_{flow} + \gamma L_{loss} \tag{12}$$

In Equation (12), L_{opt} represents the comprehensive optimization loss. L_{volt}, L_{flow}, and L_{loss} represent node voltage deviation, line load deviation, and network power loss, respectively. α, β, and γ are the corresponding weight coefficients. This loss function serves as a safety evaluation indicator for the GBD subproblem, used to determine whether the topology solution generated by the main problem satisfies the operational constraints. When the subproblem detects a constraint violation, it generates a feasible cut via the FCG mechanism and feeds it back to the main problem, thereby guiding further optimization of the network topology.

3. Results and Analysis

3.1. Performance Testing of Open Capacity Modeling Methods for Active Distribution Networks

The experiment used the IEEE 33-Bus Distribution System dataset (IEEE-33) and the National Renewable Energy Laboratory Solar Dataset (NREL Solar) as test data sources. IEEE-33 is one of the most widely used standard distribution network test systems in the field of power systems, consisting of 33 nodes, 32 lines, and multiple load nodes. The NREL Solar dataset contains data on photovoltaic irradiance, meteorological parameters, and photovoltaic power generation in multiple regions, with time resolutions covering minute and hour levels. The source website for IEEE-33 is https://matpower.org/docs/ref/matpower6.0/case33bw.html; the source website for NREL Solar is https://nsrdb.nrel.gov/. All data undergoes standardization preprocessing and is divided into an optimization scenario set and a validation scenario set in a 8:2 ratio. Specifically, the optimization scenario set is used to construct typical operating scenarios under different photovoltaic penetration rates and load levels, while the validation scenario set is used to evaluate the stability of the proposed method's capacity assessment across various operating conditions. Table 1 presents the experimental environment and its parameter configuration.

Table 1. Experimental parameter settings

Parameter	Value
Operating System	Windows 11 64-bit
CPU	Intel Core i9-13900K
GPU	NVIDIA RTX 4090 24 GB
Memory	64 GB DDR5
Simulation Platform	MATLAB R2023b + MATPOWER 8.1
Test System	IEEE 33-bus Active Distribution Network
Photovoltaic Dataset	NREL Solar Dataset
Dataset Details	2022, Phoenix, Arizona, USA; Jan.–Dec.; 1 h resolution
Photovoltaic Penetration	10%–90%, step = 2%
Load Growth Coefficient	1.0–2.5, step = 0.1
Voltage Constraint Range	0.95–1.05 p.u.
Maximum Line Loading	100%
Security Constraint	N−1 Security Criterion
Security Margin Threshold	0.15
Smoothing Coefficient η	0.6
Iterative Coefficient μ	0.5
Number of Repeated Runs	20
Evaluation Method	Average of Multiple Runs
Optimization Solver	GBD-FCG
Convergence Threshold	10^{-5}
Maximum Iterations	200

To mitigate the impact of random operational errors on experimental results, all optimization methods were independently executed 20 times, with the average result used as the final evaluation metric. For the significance analysis of performance differences among different methods, this study utilized the openable capacity improvement rates obtained from these 20 independent runs to calculate the p-value using a two-sided independent sample t-test. When p <0.05, it is concluded that the performance differences between the different methods are statistically significant. Based on two types of public datasets and the experimental settings, the sensitivity tests on key parameters were conducted for modeling the open capacity of active distribution networks. The results are shown in Figure 8.

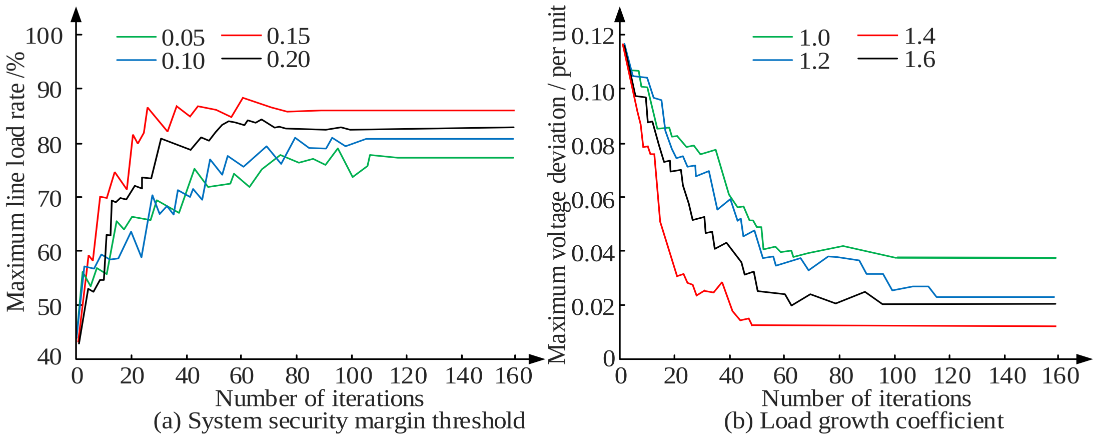

Fig. 8. Hyperparameter selection test result

Figures 8 (a) and (b) respectively show the selection test results of the system safety margin threshold ε and the load growth coefficient λ. As shown in Figure 8(a), when the system security margin threshold ε is set to 0.05,0.10,0.15, and 0.20 respectively, the maximum line load factor stabilizes at 77.8%,81.6%,86.4%, and 83.1%, respectively. It should be noted that the ε used in this paper does not represent the traditional safety margin ratio, but rather denotes the allowable range of normalized power flow deviation and voltage deviation under the N-1 fault constraint. When ε is small, the constraint conditions are more stringent, requiring the system to reserve greater operating margins, thereby limiting the available open capacity; as ε increases, the system permits a certain range of operational fluctuations, enabling the optimization model to further unleash the network's transmission capacity. However, when ε continues to increase, overly lenient security constraints may compromise the operational reliability under fault conditions; consequently, the trend of capacity enhancement gradually slows down. By comprehensively considering both the capacity enhancement capability and the safety operation requirements, this paper selects $\varepsilon = 0.15$ as the parameter for subsequent experiments. In Figure 8 (b), when the load growth coefficients were set to 1.0, 1.2, and 1.6, respectively, the maximum voltage deviation eventually stabilized at 0.038, 0.023, and 0.021 p.u. Only when the load growth factor was set at 1.4, the maximum voltage deviation reached a minimum of 0.013 p.u. and stabilized after 40 iterations, indicating that this parameter can more effectively coordinate the relationship between load growth and voltage constraints. As a result, the study ultimately set the system safety margin threshold and the load growth factor to 0.15 and 1.4, respectively.

To validate the effectiveness of the proposed method in open capacity assessment, this paper selects three typical capacity assessment methods as comparative benchmarks. Among these, the Static Capacity Method (SCM) is based on deterministic power flow analysis; it determines the maximum photovoltaic (PV) integration capacity by imposing node voltage and line capacity constraints, and thus belongs to the category of traditional deterministic capacity assessment methods; the Probabilistic Capacity Calculation Method (PCCM) accounts for the uncertainty associated with PV output and load variations; it obtains capacity assessment results at different confidence levels through probabilistic power flow analysis, thereby reflecting the impact of stochastic factors on grid integration capability [22]; and the Deterministic Voltage Margin Method (DVM) determines the capacity boundary by analyzing the relationship between node voltage margin and PV integration level, focusing specifically on how voltage constraints limit the PV integration capacity [23]. By comparing these three methods with the proposed method, this study evaluates how the maximum openable capacity varies under different PV penetration rates. The results are shown in the Figure 9.

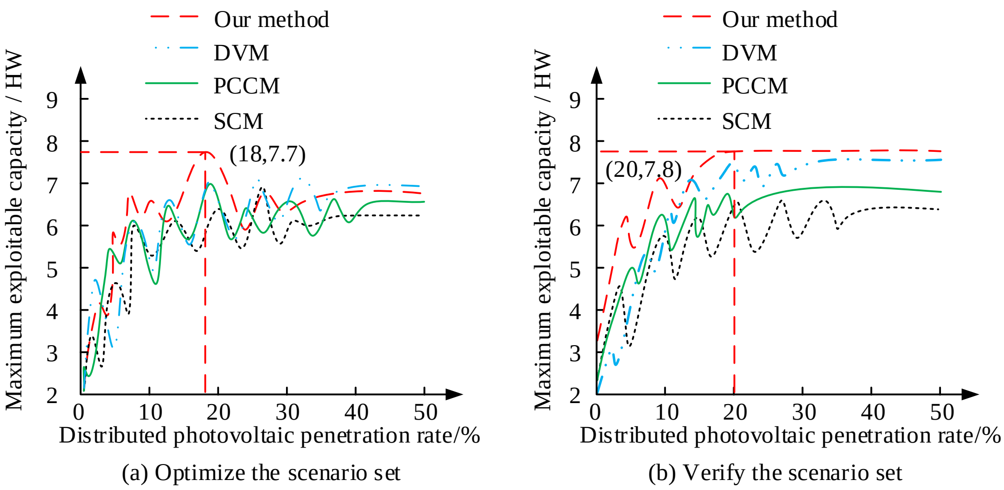

Fig. 9. Test results for the maximum developable capacity in both the training set and the test set

Figure 9(a) and Figure 9(b) respectively present the maximum available dispatchable capacity test results for each method across the optimization scenario set and the validation scenario set. As shown in Figure 9(a), the proposed method reaches a maximum open capacity of 7.7 MW at 18% PV penetration and maintains a relatively stable level thereafter. Unlike fixed-topology methods, GBD-based reconfiguration redistributes PV power among feeders, mitigating local voltage rise and reverse power flow. Figure 9(b) shows similar results for the validation scenarios, with a maximum capacity of 7.8 MW at 20% penetration, outperforming DVM, PCCM, and SCM. At higher penetration levels, capacity growth gradually saturates as line capacity and security constraints become dominant. To further analyze the impact of PV integration locations on node voltage stability, this study selects typical nodes from the IEEE 33-bus system for testing. Specifically, Node 6 serves as the near-end node, Node 18 as the central node, and Node 33 as the far-end node, representing PV integration scenarios at different electrical distances from the substation. The maximum voltage deviation, node voltage compliance rate, and number of nodes experiencing voltage violations for each method at different integration locations are presented in Table 2.

Table 2. Maximum voltage deviation results under different photovoltaic access nodes in IEEE 33-bus system

Photovoltaic access node	Method	Maximum voltage deviation / p.u.	Voltage pass rate / %	Voltage fluctuation / p.u.	Over-limit nodes
Node 6 (Near-end node)	SCM	0.043 ± 0.004	94.6 ± 1.3	0.028 ± 0.003	3
	PCCM	0.037 ± 0.003	96.2 ± 1.1	0.024 ± 0.002	2
	DVM	0.032 ± 0.003	97.4 ± 0.9	0.020 ± 0.002	1
	Our method	0.024 ± 0.002	99.1 ± 0.6	0.015 ± 0.001	0
Node 18 (Middle node)	SCM	0.051 ± 0.005	92.8 ± 1.6	0.034 ± 0.004	4
	PCCM	0.044 ± 0.004	95.3 ± 1.3	0.029 ± 0.003	3
	DVM	0.038 ± 0.003	96.8 ± 1.0	0.025 ± 0.002	2
	Our method	0.027 ± 0.002	98.7 ± 0.7	0.017 ± 0.002	0
Node 33 (Far-end node)	SCM	0.064 ± 0.006	89.5 ± 1.9	0.041 ± 0.004	6
	PCCM	0.056 ± 0.005	92.4 ± 1.6	0.036 ± 0.003	4
	DVM	0.049 ± 0.004	94.7 ± 1.3	0.031 ± 0.003	3
	Our method	0.033 ± 0.003	98.2 ± 0.8	0.021 ± 0.002	1

As shown in Table 2, for the IEEE 33-bus system, as the PV generation integration point moves from bus 6 to buses 18 and 33, the electrical distance between buses increases and the cumulative effect of line impedance intensifies, leading to an increase in voltage drop during power transmission; consequently, the maximum voltage deviation for all methods exhibits an upward trend. In the scenario where PV generation is integrated at the remote bus 33, the SCM method achieves a maximum voltage deviation of 0.064 p.u., with 6 nodes exceeding the voltage limit; in contrast, the proposed method reduces the maximum voltage deviation to 0.033 p.u. by optimizing the network topology and adjusting the power transmission path, while maintaining a voltage compliance rate of 98.2%, demonstrating that the proposed method can effectively mitigate voltage fluctuation issues induced by remote PV integration.

3.2. Verification Of Active Distribution Network Optimization and Reconfiguration Effects

The study took the IEEE 33-node active distribution network as the test object and compared the network operation status before and after reconfiguration under the distributed photovoltaic access constraints. The network topologies before and after reconfiguration were compared. The results are shown in Figure 10.

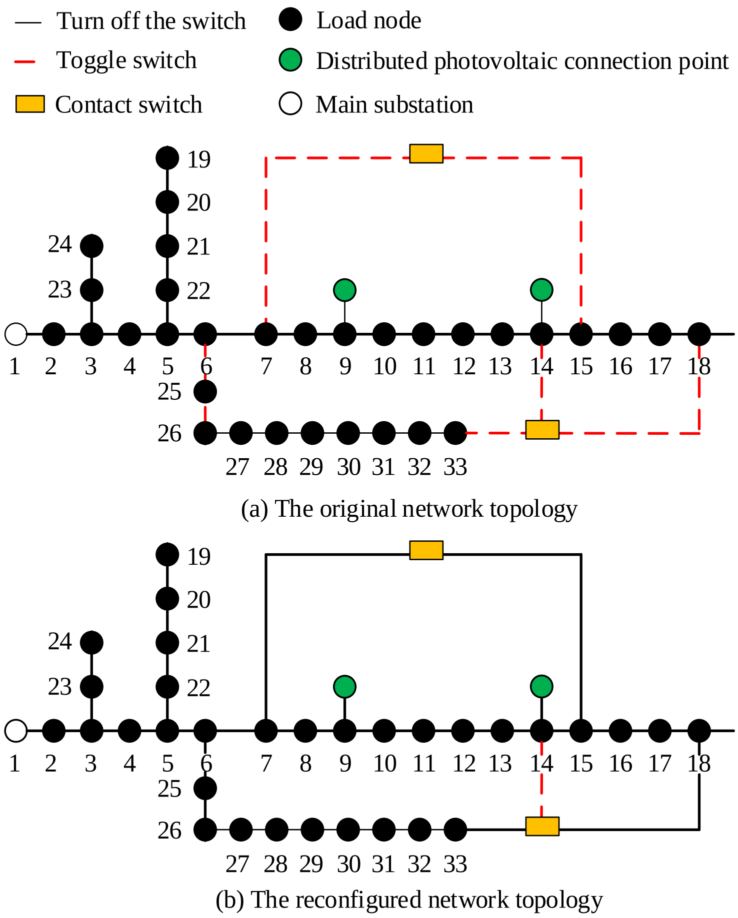

Fig. 10. Comparison results of network topology before and after reconstruction

Figures 10 (a) and (b) present the comparison results of the network topology before and after reconstruction. From Figure 10 (a), the network before reconfiguration was dominated by the original feeder structure, with the connection switch in the open state. The power transmission path between the distributed photovoltaic access point and the remote load node was long, and some branches needed to bear concentrated load transfer pressure, which easily caused problems such as uneven line load, low voltage at the end node, and local capacity limitation. As shown in Figure 10(b), the reconstructed system establishes new power flow transmission paths by closing Tie-switches 7–14 and Tie-switch 14–18, while simultaneously maintaining the radial operating structure of the distribution network through feeder switch adjustments. Specifically, the switch adjustment strategy derived from the proposed GBD-FCG method is as follows: the set of newly closed switches is {Tie-switch 7–14, Tie-switch 14–18}, and the set of newly opened switches is {S7–8, S14–15}. Here, Tie-switches 7–14 and Tie-switch 14–18 transition from their original open state to closed state to establish new power flow transmission paths; meanwhile, S7–8 and S14–15 are adjusted from closed to open state to preserve the radial operating structure of the distribution network. Compared with the original topology, the new power supply path shortens the equivalent power supply distance for certain remote nodes, enabling the power generated at photovoltaic-connected nodes to be redistributed among multiple feeders, thereby reducing local line load pressure and improving node voltage levels. To maintain the radial operating structure of the distribution network, the algorithm synchronously adjusts the states of certain feeder switches, with the specific switch changes detailed in Table 3.

Table 3. Switch status changes during network reconfiguration in the IEEE 33-bus active distribution system

Switch No.	Switch Type	Initial State	Reconfigured State	Function of Topology Adjustment
Tie-switch 7–14	Tie switch	Open	Closed	Establishes a new power transfer path and improves power distribution among feeders
Tie-switch 14–18	Tie switch	Open	Closed	Enhances voltage support capability for downstream nodes
S7–8	Sectionalizing switch	Closed	Open	Reduces local power flow concentration and maintains radial operation
S14–15	Sectionalizing switch	Closed	Open	Optimizes feeder power distribution and alleviates branch loading pressure

This study selects the Mixed-Integer Second-Order Cone Programming (MISOCP) model, the Improved Particle Swarm Optimization (IPSO) algorithm, and GBD as comparative methods; these methods are then used in conjunction with the proposed method to compute the increase rate of the openable capacity after reconstruction compared to before reconstruction; the results are shown in Figure 11.

Figures 11 (a) - (d) present the comparison results of open capacity improvement rates under each optimization method. In Figure 11 (a), MISOCP increased by 8.4%, 9.5%, 11.2%, and 13.1% respectively in low penetration, medium penetration, high penetration, and reconfiguration scenarios, with a limited overall increase. In Figure 11 (b), IPSO reached 9.2%, 10.1%, 11.3% and 14.2% respectively in the four types of scenarios, which were higher than MISOCP, but the growth was not significant in the high penetration scenarios. As shown in Figure 11 (c), GBD had an improvement rate of 15.5% in the reconfiguration scenario, but only 7.8% and 8.2% in the low and medium penetration scenarios, indicating that it is more sensitive to the initial operating conditions. As shown in Figure 11(d), the proposed method achieves capacity improvements of 9.0%,11.1%,14.2%, and 18.2% across the four scenarios, respectively, with the most pronounced improvement observed in the reconstruction scenario. To validate the differences in capacity improvement results among various optimization methods, this study employs a one-way analysis of variance (one-way ANOVA) based on 20 independent replicate runs to statistically test the capacity improvement rates of different methods; the results indicate a significant difference between the proposed method and the other comparison methods (p = 0.02). The study continued to analyze the operational status of the distribution network before and after optimization and reconfiguration, with a focus on comparing the changes in line load distribution, as shown in Figure 12. Here, the horizontal axis represents the algorithm's runtime.

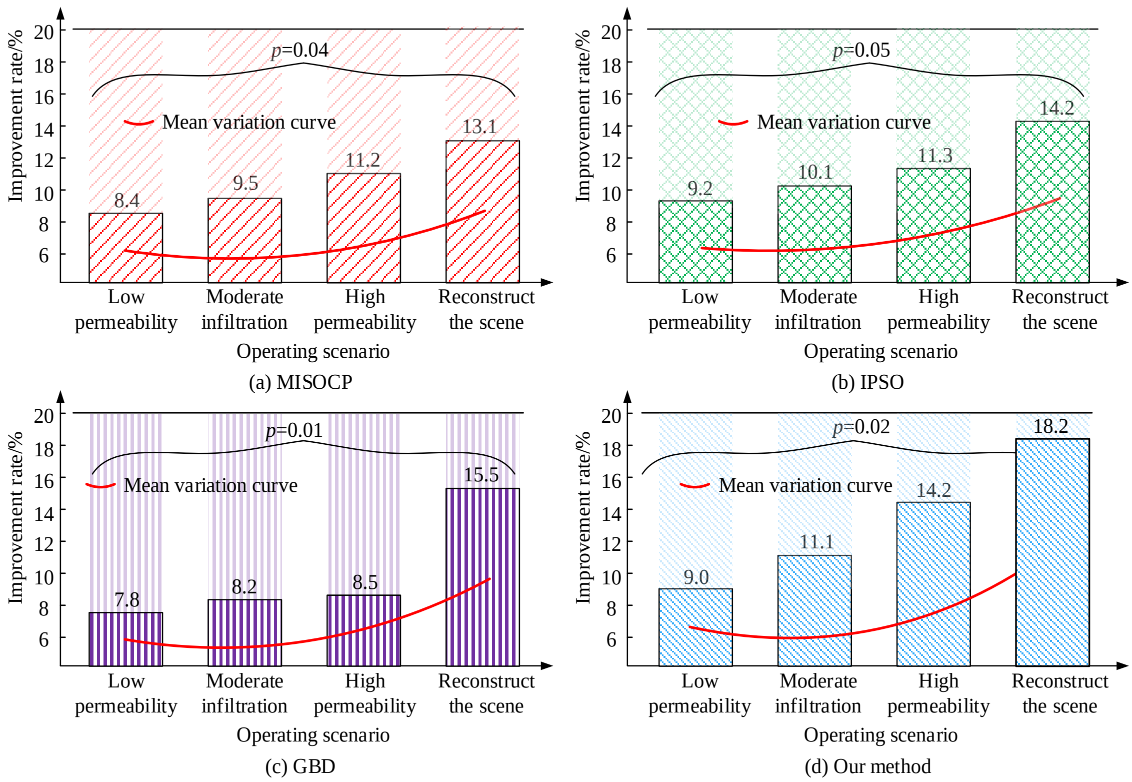

Fig. 11. Comparison of capacity improvement rates under different optimization methods

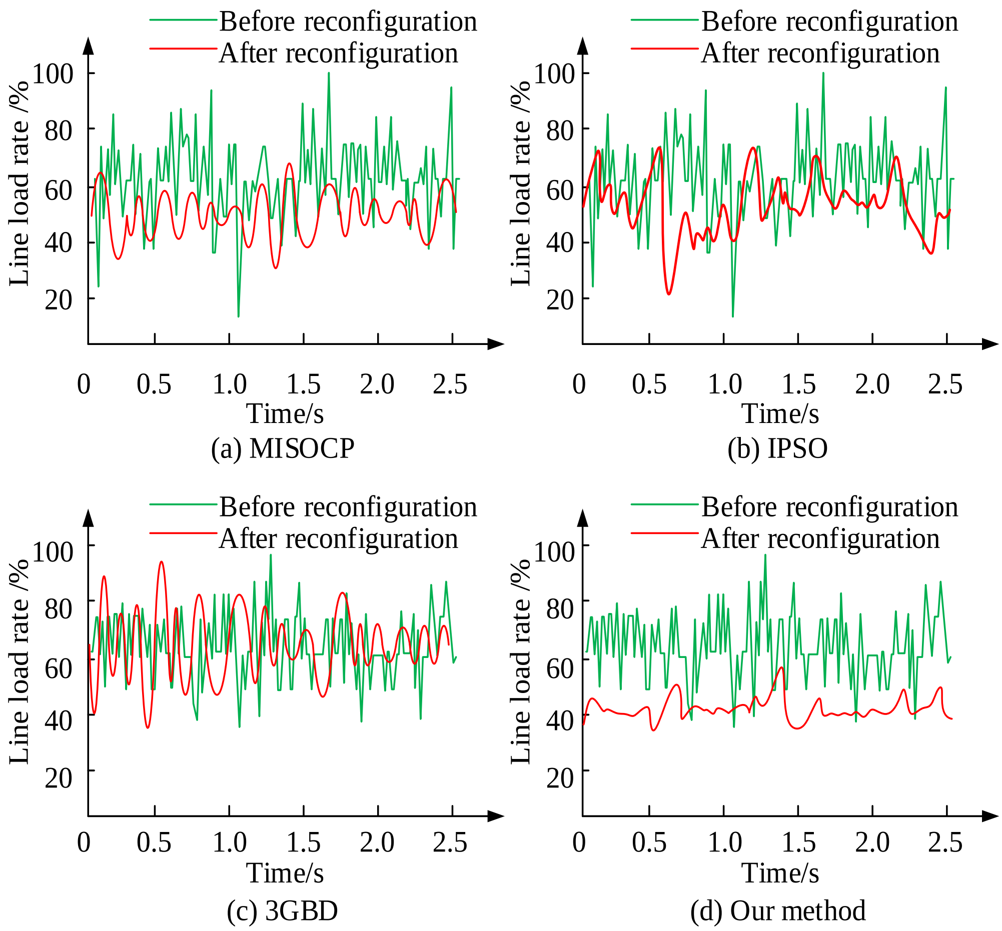

Fig. 12. Results of changes in load rates before and after the reconstruction of the route

Figures 12 (a) - (d) show the changes in line load rates for each method before and after reconstruction. In Figure 12 (a), the average line load rate after MISOCP reconstruction decreased from 64.8% to 52.6%, but the peak still reached 72.4%, indicating that it can reduce the load pressure of some lines, but the suppression effect on local heavy load is limited. In Figure 12 (b), the average line load rate after IPSO reconfiguration decreased from 66.3% to 50.7%, and the peak decreased to 68.5%. The load reduction effect was better than that of MISOCP. In Figure 12 (c), the average line load rate after GBD reconstruction decreased from 65.9% to 61.4%, and the peak still reached 83.7%, indicating its insufficient load distribution capacity under complex conditions. As shown in Figure 12 (d), the average line load rate after reconstruction by the proposed method decreased from 67.2% to 43.6%, the peak decreased from 89.4% to 54.8%, and the fluctuation range was significantly smaller than that of other methods. Overall, the proposed method can more effectively reduce the peak line load, lower the average load level, and improve the operational stability of the active distribution network. However, a reduction in line load factor does not imply a decline in grid operational efficiency. Since the reconfiguration process simultaneously incorporates both the enhancement of available open capacity and system loss constraints, the optimized topology can mitigate high-loss operating conditions resulting from local line overloads. Specifically, the redistribution of line loads leads to a more balanced current distribution and reduces line resistance losses, thereby enhancing the grid's photovoltaic integration capability while maintaining an optimal economic operational level. Consequently, the proposed method facilitates a transition from localized high-load operation to a globally balanced grid operation, rather than merely reducing line utilization rates. Finally, the study tested the convergence performance and computing time of the algorithm in different scenarios, as presented in Table 4.

Table 4. Algorithm convergence performance and computation time under different scenarios

Scenario	Method	Convergence iterations	Computation time / s	Optimal capacity / MW	Peak memory usage / GB
Low load (λ=1.1, 110% of base load)	MISOCP	43	12.3	7.8	2.84
	IPSO	36	9.8	8.1	2.31
	Standard GBD (without FCG)	29	11.5	8.6	1.96
	Our method	25	7.4	9.2	1.62
Medium load (λ=1.4, 140% of base load)	MISOCP	52	14.6	8.2	3.12
	IPSO	41	11.3	8.6	2.55
	Standard GBD (without FCG)	33	13.1	9.1	2.14
	Our method	27	8.2	9.7	1.79
High load (λ=1.8, 180% of base load)	MISOCP	61	18.3	8.7	3.56
	IPSO	47	13.8	9.1	2.88
	Standard GBD (without FCG)	38	15.7	9.5	2.43
	Our method	29	9.6	10.3	2.01
Extreme load (λ=2.5, 250% of base load)	MISOCP	70	21.5	9	4.08
	IPSO	53	16.2	9.4	3.24
	Standard GBD (without FCG)	42	17.9	9.8	2.76
	Our method	31	10.8	10.7	2.28

Note: Standard GBD denotes the conventional generalized Benders decomposition method without the feasible cut generation (FCG) mechanism, whereas Proposed GBD-FCG denotes the method developed in this study.

As shown in Table 4, under low-load scenarios, the proposed method requires only 25 iterations with a computation time of 7.4 seconds and achieves a maximum controllable power output of 9.2 MW, demonstrating superior overall performance compared to both MISOCP and IPSO. In extreme load scenarios, the proposed method takes 10.8 seconds for computation and achieves a maximum controllable power output of 10.7 MW, while maintaining a fast convergence speed. It should be noted that this computation time is primarily allocated to the network reconfiguration decision-making process during the offline optimization phase; however, in actual active distribution network operations, day-ahead or rolling optimization strategies are typically employed. Therefore, the second-level computation time adequately meets engineering application requirements. Meanwhile, although MISOCP belongs to the class of convex optimization models, its solution process still involves addressing a complex integer combinatorial search problem due to the presence of numerous discrete switch variables and nonlinear security constraints within this problem formulation. As the load level increases, both the model size and the number of constraints expand further, leading to increased computation time. In contrast, the GBD-FCG method decomposes the master problem and subproblems and employs a feasible cut generation mechanism to reduce the ineffective search space, enabling it to achieve faster convergence speeds and higher capacity optimization results even in complex scenarios.

4. Summary

Research has demonstrated that the proposed active distribution network-based method for modeling and optimizing renewable energy integration capacity—which incorporates constraints arising from distributed photovoltaic (PV) systems—can effectively address challenges such as inaccurate capacity assessments under high PV penetration scenarios, difficulties in handling reverse power flow constraints, and suboptimal efficiency in network topology optimization. By constructing a capacity assessment model that integrates PV integration constraints, voltage security constraints, line transmission constraints, and N–1 security constraint, and by combining this model with a collaborative optimization mechanism involving GBD and FCG, this approach achieves efficient coordination between the discrete network topology decision-making process and the continuous power flow verification process.

The parameter sensitivity analysis demonstrates that an appropriate selection of the safety margin threshold and the load growth coefficient can effectively balance system security with capacity release capability. Specifically, when the safety margin threshold is set to 0.15 and the load growth coefficient is set to 1.4, the maximum line load ratio of the system reaches 86.4%, while the maximum voltage deviation is reduced to 0.013 p.u. These results indicate that the proposed GBD-FCG optimization framework can effectively coordinate voltage stability, line transmission capacity, and capacity enhancement objectives under complex active distribution network constraints; by reducing the search space for infeasible topologies, it enhances the global optimization capability of the optimization process, rather than relying solely on parameter adjustments to achieve performance improvement.

In tests conducted at various PV integration locations, the proposed method effectively mitigates the voltage fluctuation risks induced by high penetration of photovoltaic (PV) generation. Particularly in remote node integration scenarios, the maximum voltage deviation is controlled within 0.033 p.u., with a voltage compliance rate reaching 98.2%, demonstrating that the constructed model accurately captures the coupling effects among PV integration locations, changes in power flow directions, and network constraints. In the network reconfiguration experiments, the proposed method achieves an increase in available capacity of 18.2%, reduces the average line load factor from 67.2% to 43.6%, and lowers the peak load factor from 89.4% to 54.8%. These results indicate that the reconfiguration process not only enhances the curtailment capability of distributed PV systems but also reduces the risk of prolonged high-load operation on local transmission lines, thereby helping to minimize line thermal losses, alleviate equipment operational stress, and reduce long-term O&M costs for distribution networks. Furthermore, under extreme load conditions, the proposed method achieves a maximum available capacity of 10.7 MW after only 31 iterations, with a computation time of 10.8 seconds. Compared with traditional metaheuristic online reconfiguration methods, these results demonstrate that the GBD-FCG method achieves superior computational efficiency while maintaining optimal capacity optimization performance, making it particularly suitable for topology adjustment requirements in active distribution networks for day-ahead dispatching and rolling optimization scenarios.

However, current models primarily focus on optimizing scenarios involving typical photovoltaic (PV) grid integration and single fault constraints; they still exhibit certain limitations in terms of dynamic adaptability under extreme PV rapid fluctuations or situations where multiple faults occur simultaneously. When the PV output undergoes abrupt changes within a short time frame, the uncertainty in nodal power injection may lead to rapid shifts in the original feasible region, thereby increasing the information feedback frequency between the GBD master problem and its subproblems, while reducing the efficiency of FCG constraint generation; concurrently, the superposition of multiple faults may render traditional N–1 security constraints inadequate for accurately describing the system's risk boundary. Future research could further integrate energy storage systems, dynamic reactive power compensation devices, and multi-time-scale forecasting models into the existing GBD framework—by treating energy storage charging/discharging strategies and reactive power regulation processes as subproblem constraint variables—to achieve a synergistic solution for capacity optimization, dynamic regulation, and security control, thereby further enhancing the robustness of active distribution networks under complex operating conditions.

Symbol-to-Abbreviation Reference Table

i, j : Distribution network node index

l : Distribution line index

t : Time state index

N : Total number of distribution network nodes

L : Distribution line set

P_i^G : The active power supply provided by the substation to node i

P_i^{PV} : Active power injection of node-based distributed photovoltaic systems

P_i^L : Node load power consumption

V_i, V_j : Node voltage magnitude

G_{ij}, B_{ij} : The conductance and susceptance of the node admittance matrix

θ_{ij} : Node phase angle difference

Q_i^G, Q_i^{PV}, Q_i^L : Substation reactive power support, photovoltaic system reactive power injection, and node load reactive power demand

F : Maximum system openable capacity

λ : Load growth factor

$\frac{\partial V_i}{\partial P_i^{PV}}$: Sensitivity coefficient of node voltages to changes in photovoltaic power output

ΔP_i^{PV} : Incremental photovoltaic power output

$V_i^{\min}, V_i^{max}$: Voltage upper and lower limits

P_{ij}, Q_{ij} : Line active power and reactive power

S_{ij}^{max} : Maximum allowable transmission capacity of the line

S_{ij}^k : The apparent power flow of line $i - j$ in the k type of fault scenario

S_{ij}^{max} : The maximum transmission capacity allowed for Line $i - j$

V_i^k : The voltage amplitude of node i in the first fault scenario k

V_i^{ref} : Node rated voltage

ε : System safety margin threshold

Z : Comprehensive optimization objective

ω_1, ω_1 ; Capacity weight and loss weight coefficient

ω_1, I_{ij} : Line resistance and line current

X_{ij} : Line $i - j$ reactance

θ_i, θ_j : The voltage phase angle between node i and node j

x : Network switch state decision variable in the main problem

x^k : The switching state obtained in the kth iteration

$g(x^k)$: The first-order gradient information of the constraint function at the current iteration point

$P_i^{PV,opt}$: Optimized PV grid-connection capacity

$Z^{(t)}$: The optimization target value of the t -th iteration

L_{opt} : Comprehensive loss optimization

$L_{volt}, L_{flow}, L_{loss}$: Node voltage deviation, line load deviation, and network power loss

α, β, γ : Weight coefficient

References

[1] Hadi H A, Kassem A, Amoud H, Nadweh H, Ghazaly S, Moubayed N M. Using active filter controlled by imperialist competitive algorithm ICA for harmonic mitigation in grid-connected PV systems. International Journal of Robotics and Control Systems, 2024, 4(2): 581-605. https://doi.org/10.31763/ijrcs.v4i2.1365

[2] Pratap A, Tiwari P, Maurya R. Simultaneous optimal network reconfiguration and power compensators allocation with electric vehicle charging station integration using hybrid optimization approach. Electrical Engineering, 2025, 107(3): 2935-2967. https://doi.org/10.1007/s00202-024-02630-2

[3] Othman A F, Othman M L, Ab Kadir M Z A, Wahab N I Z, Wahab A A Z A, Yusoff W Y W, Hadi M K. Optimal Distribution Network Reconfiguration via the Integration of Distributed Generation Penetration using Meta-Heuristic Technique. Journal of Advanced Research Design, 2026, 139(1): 101-118. https://doi.org/10.37934/ard.139.1.101118

[4] Lu L, Xu H, Ma H, Lu Y, Li Y. Distribution Network Reconfiguration Based on Collaborative Optimization Including Source-Load Uncertainty and Demand Response with Energy Storage Access. Journal of Electrical Engineering & Technology, 2025, 20(8): 5021-5038. https://doi.org/10.1007/s42835-025-02368-2

[5] Tian B, Guo Z, Zhou B, Fan L, Deng Z, Zhang Y, You Z, Lin L. A distributed model-free adaptive voltage control algorithm for distribution systems with extensive integration of photovoltaics. Energy Conversion and Economics, 2025, 6(1): 54-63. https://doi.org/10.1049/enc2.70003

[6] Liu S, Jia Z, Liu T. Ensuring resilience in active distribution networks: A security-constrained robust approach with energy storage and demand response. Journal of Computational Methods in Sciences and Engineering, 2025, 25(2): 1702-1713. https://doi.org/10.1177/14727978241302984

[7] Yang X, Li Z, Ding L, Hu Z, Fang H. Reconfigurable converter-formed soft open point-assisted dynamic restoration for distribution systems with cold-load pickup. IEEE Transactions on Sustainable Energy, 2025, 16(4): 2271-2285. https://doi.org/10.1109/TSTE.2025.3532911

[8] Papastergiou S, Basheer N, Lampropoulos K, Verrios P, Islam S. Explainable AI based dynamic cybersecurity risk management for cyber insurability: S. International Journal of Information Security, 2026, 25(1): 36-44. https://doi.org/10.1007/s10207-025-01189-8

[9] Elumalai G, Lakshmanan M, Tapas Bapu B R, Srilakshmi K. Hybrid IMAO–IBESO optimization approach for the best location of EV charging stations in active distribution networks. Electrical Engineering, 2026, 108(3): 203-208. https://doi.org/10.1007/s00202-026-03541-0

[10] Oni O M, Omirinlewo A B, Balogun O E, Efiong J E, Afolabi A, Olajubu E A. A Predictive Framework for Dynamic Risk Management in Industrial Control System Networks. Journal of Future Artificial Intelligence and Technologies, 2026, 3(1): 167-193. https://doi.org/10.62411/faith.3048-3719-348

[11] Chowdhury A, Roy R, Mandal K K. Sustainability and Capacity Estimation of Photovoltaic Based Distribution Network Integrated with Demand Response Using Arithmetic Optimizer Algorithm. Iranian Journal of Science and Technology, Transactions of Electrical Engineering, 2025, 49(1): 197-226. https://doi.org/10.1007/s40998-024-00762-6

[12] Khodr H M, Martinez-Crespo J, Matos M A, Pereira J. Distribution systems reconfiguration based on OPF using Benders decomposition. IEEE Transactions on Power Delivery, 2009, 24(4): 2166-2176. https://doi.org/10.1109/TPWRD.2009.2027510

[13] Tavagnutti A A, Vicenzutti A, Chiandone M, Bosich, D, Sulligoi G. The digital twin of complex shipboard DC microgrids: The high-performing synergy of compiled models and HIL platform in the dynamics emulation of zonal power electronic power distribution systems. IET Power Electronics, 2025, 18(1): 12835-12884. https://doi.org/10.1049/pel2.12835

[14] Ahmed E E E, Demirci A, Poyrazoglu G, Manshadi S D. An equitable active power curtailment framework for overvoltage mitigation in PV-rich active distribution networks. IEEE Transactions on Sustainable Energy, 2024, 15(4): 2745-2757. https://doi.org/10.1109/TSTE.2024.3442834

[15] Nuamkoksung P, Sanga-ngam W, Suthumno K. Integrated Control of DER Placement and Network Reconfiguration in EV-Charging Distribution Systems Using Multi-Optimization Techniques. Engineering Access, 2025, 11(2): 301-318. https://doi.org/10.14456/mijet.2025.31

[16] Cikan M, Cikan N N, Kekezoglu B. Determination of optimal island regions with simultaneous DG allocation and reconfiguration in power distribution networks. IET Renewable Power Generation, 2025, 19(1): 12942-12948. https://doi.org/10.1049/rpg2.12942

[17] Cikan M. Multi-objective approaches for optimizing 37-bus power distribution systems with reconfiguration technique: from unbalance current & voltage factor to reliability indices. Computer Modeling in Engineering & Sciences, 2025, 143(1): 673-721. https://doi.org/10.32604/cmes.2025.061699

[18] Gupta R K, Fahmy S, Chevron M, Vasapollo R, Figini E, Paolone M. Grid-aware scheduling and control of electric vehicle charging stations for dispatching active distribution networks: Theory and experimental validation. IEEE Transactions on Smart Grid, 2025, 16(2): 1575-1589. https://doi.org/10.1109/TSG.2025.3526477

[19] Jaradat T, Khatib T. Optimal sizing of battery energy storage system in electrical power distribution network. Energy Exploration & Exploitation, 2025, 43(3): 909-931. https://doi.org/10.1177/01445987241300183

[20] Subramanian B K, Fetu M, Mulugeta B. Optimization of distribution network reconfiguration for power loss minimization using GOA: a case study of Dilla substation, Ethiopia. Engineering Research Express, 2025, 7(2): 25377-25381. https://doi.org/1088/2631-8695/adcdc5

[21] Shelar D, Amin S, Hiskens I A. Evaluating resilience of electricity distribution networks via a modification of generalized benders decomposition method. IEEE Transactions on Control of Network Systems, 2021, 8(3): 1225-1238. https://doi.org/10.1109/TCNS.2021.3061671

[22] Geoffrion A M. Generalized Benders Decomposition. Journal of Optimization Theory and Applications, 1972, 10(4): 237-260. https://doi.org/10.1007/BF00934810

[23] Baran M E, Wu F F. Network reconfiguration in distribution systems for loss reduction and load balancing. IEEE Transactions on Power Delivery, 1989, 4(2): 1401-1407. https://doi.org/10.1109/61.25627